Article

Dynamic Load Test and Contact Force Analysis of the AERORail Structure

Fangyuan Li [1,*], Zhenwei Guo [1], Yunxuan Cui [2] and Peifeng Wu [1]

[1] Department of Bridge Engineering, College of Civil Engineering, Tongji University, Shanghai 200092, China
[2] School of Civil and Environmental Engineering, University of New South Wales, Sydney, NSW 2052, Australia
* Correspondence: fyli@tongji.edu.cn

Abstract: The flexible structure of the new type of aerial track studied in this paper is formed by strings and tracks, which have obvious dynamic characteristics under the action of vehicle moving loads and is also an important factor affecting its performance. The paper uses the full-scale model of AERORail, based on the modal test under a specific span, combined with the fundamental frequency analysis of the structure, and carries out the dynamic load test to determine the change law of the contact force acting on the rail by the dynamic load. The time-domain improved algorithm based on the method of moments is used to identify and analyze the dynamic loads under different spans and vehicle speeds and to determine the correlation between the dispatched loads and the spans and vehicle speeds. It is proven that the occurrence time and frequency of the contact force are related to the passing time of the vehicle. The contact force fluctuates with the change in the vehicle speed, but with the increase in the span, the fluctuation of the contact force decreases obviously. The relevant conclusions provide support for the layout of the AERORail vehicle load. For this innovative structure, the relevant conclusions provide the basis for the application of this novel structure.

Keywords: dynamic load; AERORail; flexible structure; full-scale model; vehicle-rail coupling; moving load; fundamental frequency; contact force

1. Introduction

The AERORail Transportation System referred to as AERORail, is a new type of transportation system in the form of a cable-supported rail combined structure (see Figure 1) composed of multispan continuous string cables, rails, lower supports and related power supply and control systems [1]. Similar to existing top-supported suspension bridges or stress zone bridges, the typical projects include the Rio-Colorado Suspension Bridge in Costa Rica (108 m in span), the Bad Sand Bridge on the Elbe River in Germany (100 m in span), Su Rifeng Bridge (48 m in span) in central Kyushu, Japan and Taojin Bridge (74 m in span) in Taojin Village, Dongkou County, Hunan, China [2,3].

The AERORail structure uses steel as the structural material, replacing the use of concrete and prestressed concrete in the superstructure; it cancels the heavy superstructure in traditional bridges and forms a common stress system directly formed by the rail and the string cable, which is a veritable hollow structure in the sky; its structural rigidity mainly comes from the stress rigidity generated by the prestressing of the string cable [4]. Due to its obvious structural flexibility characteristics, its structural dynamic characteristics are the focus of research and important structural characteristics that must be mastered in the future application process. The problem corresponding to the characteristics of its flexible structure is that when it is subjected to moving loads, the force and deformation, and vibration and stability of the structure have obvious coupling effects between the structure and the moving loads.
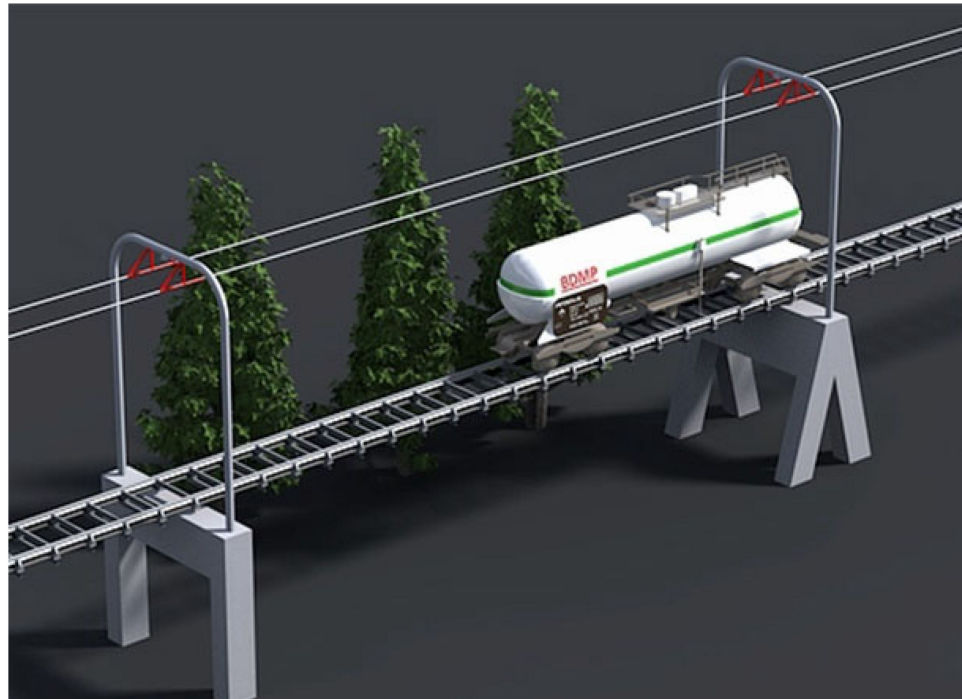
Figure 1. Schematic diagram of the typical structure of AERORail.

As a flexible structure, its structural form is somewhat similar to that of string beams. The biggest difference from conventional string beams used in buildings is that AERORail is simpler in structure, and the overall structural size is more represented as a longitudinal one-dimensional structure, even in the lateral direction, showing that the lateral dimension is much larger than the height dimension [5]. Second, the servicing load on the AERORail is a moving load, and the load causes the structure to deform considerably when it is no-load and full-load [6]. Therefore, from the stress point of view, the AERORail structure is more like a stress ribbon structure.

For such light and flexible structures with pretensioned cables, Zhao [7] studied the prestressing process, and most typical experimental studies are represented, including both full-scale tests and downscale orthogonal tests. The static behavior and the effect of a prestressed cable on structural stability are presented, followed by a typical full-scale static loading test with dynamic behavior, such as the natural vibration characteristics. Based on the structural characteristics of a tensioned string bridge, Zhou [8] used the Rayleigh method to derive formulas for calculating the frequencies of vertical, antisymmetric and lateral bending vibrations. Stefan Hartweg and Andreas Heckmann [9] derived the kinematics and governing equations of motion of a general flexible multibody system and their extension to moving loads and presented a method to handle discontinuities when moving loads separate from the flexible structure. Zhou [8] studied the dynamic structural characteristics of a tensioned string bridge based on the Rayleigh method to derive formulas for calculating the frequencies of vertical, antisymmetric and lateral bending vibrations. He found that the shape and physical characteristics of the main cable have a greater impact on the vertical symmetrical vibration frequency than the lateral bending frequency, and the vertical bending symmetrical vibration frequency increases with an increasing rise-to-span ratio. The tension force of the main cable has no influence on the frequency of tensioned string bridges. The first-order frequency of the tensioned string bridge is generally the vertical bending symmetrical vibration frequency. The fundamental frequency of a structure can be greatly increased, thereby increasing the overall rigidity of the structure. Lee [10] studied a numerical method for the dynamic analysis of vehicles moving on flexible structures with gaps and gained the dynamic contact between a high-speed wheel and elastic beam with Coulomb friction [11]. Zhao [12] studied the dynamics and stability of slender structures

carrying a moving load or mass with FEM. Xiao [13] studied the vibration control of stress ribbon bridges subjected to moving vehicles.

Based on the above structural characteristics, AERORail not only has the static and dynamic characteristics of the conventional flexible beam structure but also the vibration and stability under the action of the moving load are closer to the stress ribbon structure [13–15]. The difference is that the AERORail load acts directly on the rail on the upper part of the prestressed cable and is then transmitted to the cable through the support rod, which is similar to the top-supported suspension cable structure. To ensure the efficiency of AERORail transportation, the support between the cable and the track is not as high as that of the top-mounted suspension cable structure; that is, the catenary span of the cable is relatively small. The rise span ratio is between 1/100 and 1/50, which causes AERORail to look more like a truss with cables parallel to the rail from a distance.

At present, research on AERORail structures mainly focuses on the static and dynamic characteristics of the structure. Li [4,16] used 1:20 and 1:15 scale models to preliminarily verify the feasibility of the AERORail structure and used the virtual prototype to explore the dynamic and static characteristics of the structure [16]. Numerical analysis of the static deflection of different spans of AERORail under different loads and pretensions was carried out, and the 1:1 full-scale AERORail test was used for verification (Figure 2); the relevant results have been carried out in a special report in China Central Television and China Education Television. At the same time, on this basis, combined with vehicle-bridge coupling theory, the dynamic deflection response of AERORail with different spans is studied, and some useful conclusions are obtained.

Figure 2. Full-scale model test line.

Existing studies have shown that under the action of low-speed moving loads, the cable stress increment, dynamic deflection and structural stiffness of the AERORail structure do not change significantly; with the increase in cable force and mid-span support height, the structural stiffness increases significantly. There is a nonlinear relationship with dynamic deflection [17,18].

Although some studies have initially revealed some of the static and dynamic characteristics of the AERORail structure, for engineering applications of related research, these results still cannot satisfy the establishment of relevant design theories and design methods. At present, there are still problems that need to be studied urgently including the static

and dynamic characteristics of the long-span AERORail structure, the dynamic response of the AERORail structure under high-speed driving conditions, the vehicle-AERORail interaction, and the practical calculation method of the static and dynamic response of the AERORail structure.

Based on the existing research results, this paper studies the force between the vehicle and the AERORail structure—the wheel-rail contact force. On the basis of the modal test, the fundamental frequency of the structure is determined. Then the research on the vehicle-rail force under the condition of the vehicle load determines the stability and control requirements during the service of the AERORail and provides a theoretical basis for the design of the structure in the future, especially the arrangement of the vehicle load on the track line. It is also an important guarantee to ensure the safety and usability of the structure.

2. AERORail Test Line with Modal Test

Existing numerical simulations have preliminarily verified the availability and reliability of the dynamic model calculation method and identification algorithm. To verify the reliability of the application of this theoretical system to the study of AERORail structures and to provide a basis for the subsequent calculation of the real vehicle-rail contact force, it is necessary to conduct verification tests by means of model tests.

Commonly used structural test methods include small-scale model tests and full-scale model tests. Due to the high cost of full-scale models, they are generally difficult to achieve. For the study of the new structure of AERORail, considering the particularity of the structure, the author realized the construction of the full-scale rail so that the conditions under the actual application state can be used to carry out the test, and the measured data under the real conditions can be obtained. The long-term significance is also helpful for future research on AERORail vibrating absorption and stability control. This paper is the relevant research work carried out by using the 1:1 AERORail structure test line.

2.1. Test Line Structure

The AERORail test line adopts a steel structure as a whole, and the substructure adopts a steel column support and concrete foundation. The main components of the AERORail structure include rails, cables, struts, piers, lateral connections and anchorages [17,18]. The general layout of the AERORail test line used is shown in Figure 3.
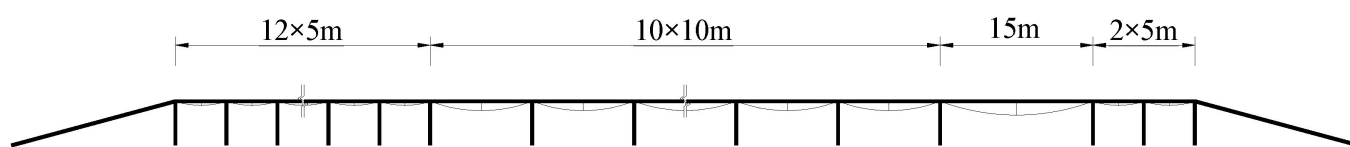
**Figure 3.** General layout of the AERORail test line.

Both ends of the test line are anchored, and the left side is the starting point of the moving load. The span layout adopts the scheme of 12×5 m + 10×10 m + 15 m + 2×5 m, and the total length is 203 m (including the slope at both ends, excluding the anchorage). By removing the support of the 10 m span in the middle part of the test line, the combined arrangement of 10 m, 20 m and 30 m spans is realized so that the span arrangement with a modulus of 5 m is realized in the whole line.

2.1.1. Superstructure of the Test Line

The track adopts a 43 kg/m standard section rail, and its section parameters are shown in Figure 3 and Table 1. The cable components are $\phi15.24$ steel strands, with 5 cables on one side and two bundles in total, arranged under the rail. The horizontal spacing of the rails is 1.5 m, and a horizontal tie rod is arranged every 5 m in the longitudinal direction as a horizontal connection. The standard span layout is shown in Figure 4.

Table 1. Summary of the height of each span strut.

Span Number	1~12	13~22	23		24~25
span(m)	5	10	15		5
pole position	mid-span	mid-span	mid-span	quarter point	mid-span
strut design length (mm)	100	200	340	200	100
actual length of strut (mm)	100	206~210	340~341	208~210	100
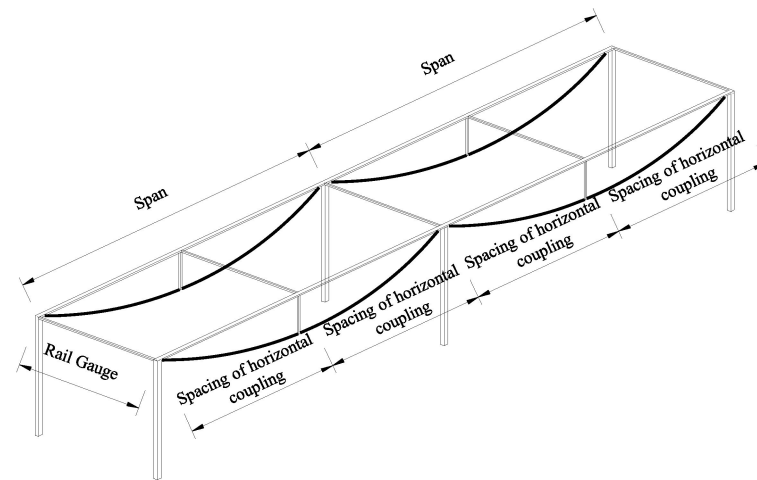
Figure 4. Schematic diagram of the segment of the AERORail test line.

A single transverse connecting rod is composed of steel pipes and clamps at both ends. At the position of the pier column, the bowl buckle clamp is used to buckle the top of the pier column; in the position without the pier column, the claw clamp is used to buckle under the rail. Through preliminary tests, it is determined that the vertical spacing of horizontal couplings should not be too large or too small. Too small a spacing will lead to a waste of material, while too large a spacing will make the overall structure and even the track out-of-plane unstable; too large a spacing may also lead to unbalanced load distribution on both sides of the structure. According to the finite element analysis of the upper load, the horizontal arrangement of the free length of the track is approximately 5~8 m. The vertical strut is designed with the support plate and the steel pipe, and its total length is determined according to the shape of the cable and the position of the support.

In this test line, the pole-support heights used for cables with different spans are shown in Table 1 below:

At the top of the pier, the cable needs to pass through the reserved channel, and there is a certain angle. When the cable is prestressed and loaded with live load, a certain slip occurs here, which is similar to the slip of the main cable of a suspension bridge when the bridge is completed. This kind of sliding plays a very important role in balancing the force and prestress of the two adjacent spans; the appropriate structural measures should be used to ensure sliding instead of a fixed restraint to reduce the effect of horizontal force on the support column and its instability. In addition, because the edge of the steel member tunnel itself is difficult to ensure smoothness, and its edges and corners form local stress concentration on the cable body, it is very easy to damage the cable body, so structural measures should be taken to solve it. To solve these two problems, this test line uses the construction method of laying tetrafluoroethylene sliding plates in the tunnel to address the tunnel on the top of each pier.

2.1.2. The Substructure of the Test Line

The piers of the test line are made of steel pipes, and the lower part of the column is connected with the embedded parts in the concrete foundation by bolts; between the two piers in the north and south of the test line, bowl-type fasteners and a pair of steel pipes are used to form X braces (see Figure 5).To ensure the lateral stiffness and stability of the structure, at the piers with variable slope spans, additional diagonal braces are set to reinforce and support the columns horizontally and vertically.


Figure 5. AERORail structure and support picture.

2.2. Modal Test

Modal analysis is the premise and foundation of the dynamic analysis of linear elastic structures. Although in most cases the modal parameters calculated by using the finite element model can meet the needs of engineering applications, for the study of new structures the structural modal parameters (modal frequency, modal shape and modal damping, etc.) verification research methods are fundamental work and very necessary [19–21]. The modal test and analysis of the five-pole supported AERORail structure with a span of 30 m are used to verify the correctness of the finite element modal analysis method and obtain more real modal parameters.

The 30 m span and five-pole supported AERORail selected for the model test are provided with a set of supports at 1/6, 1/3, 1/2, 2/3 and 5/6 of the span, and the five-pole support heights are 21.5 cm, 52 cm and 62 cm, 52 cm and 21.5 cm, respectively (see Figure 6).
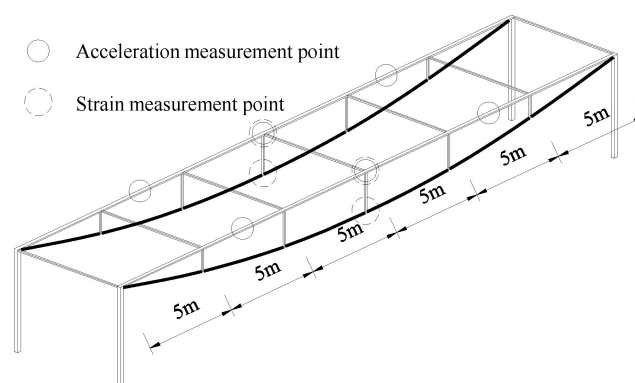
Figure 6. Schematic diagram of the 30 m span AERORail supported by 5 poles.

Since the modal frequency of the AERORail structure is directly related to the cable force, the cable strain is also measured in the modal test and finally used to calculate the actual cable force. After measurement and calculation, the cable force on the north and south sides is 30.2 kN.

The modal analysis uses frequency domain decomposition to calculate modal frequencies and modal shapes [8,22], the modal damping ratio is determined by the half-power bandwidth method, and the excitation method is hammer excitation [21]. After analysis and calculation, the modal parameters of the 30 m-span five-pole supported AERORail structure are shown in Table 2.

Table 2. Modal parameters of 30 m span and five support AERORail.

		First Order		Second Order		Third Order	
		Vertical	Horizontal	Vertical	Horizontal	Vertical	Horizontal
frequency (Hz)	north	1.57	2.51/4.7	-	6.27	4.86	7.99
damping ratio (%)		3.72	2.12	-	-	2.62	6.31
frequency (Hz)	south	1.57	0.78	-	6.27	4.86	2.51/4.7
damping ratio (%)		3.72	-	-	-	-	-

The item "-" in the table is not detected.

According to the actual structure of the 30-m-span structure, calculated by the finite element model, the transverse modal frequencies are 0.49 Hz, 1.15 Hz and 2.09 Hz, and the vertical modal frequencies are 1.17 Hz, 1.90 Hz and 4.26 Hz.

The modal test and analysis results (Figure 7) show that the vertical vibration mode obtained by the finite element analysis is basically the same as the vibration mode of the AERORail structure, but there is a certain error in the modal frequency, which is approximately 10%~20%. Transverse modes have large errors (over 100%) in both mode shape and frequency. This is because the real structure is a multispan structure transversely, and there is no transverse constraint. Therefore, under the support of the current research results, the modal parameters of the finite element model can be used for the vertical vibration analysis of AERORail, while the lateral vibration needs to be further studied.


(**a**)　　　　　　　　　　　　　　　　　　　　　　　　(**b**)
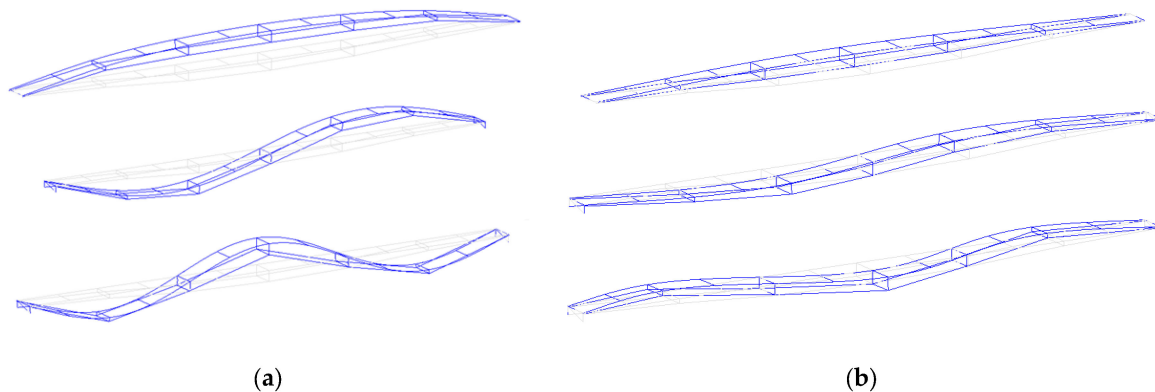
Figure 7. Finite element mode shape diagram. (**a**) Vertical mode, (**b**) Transverse mode.

3. AERORail Dynamic Load Test and Analysis

3.1. Structural Fundamental Frequency

Whether it is an improved time domain algorithm based on the method of moments or an original time domain identification algorithm [23], all require a series of basic parameters including the fundamental frequency of the structure to be obtained in advance. In this paper, the finite element method is used to establish models of three spans (Figure 8) and calculate the fundamental frequency of the structure. To accurately reflect the dynamic characteristics of the structure, the following three structural features were mainly considered in the modeling: the tensile force of the cable provides additional stiffness; the slippage of the cable in the channels at both ends of the single span and the size of the strut in the middle of the span.
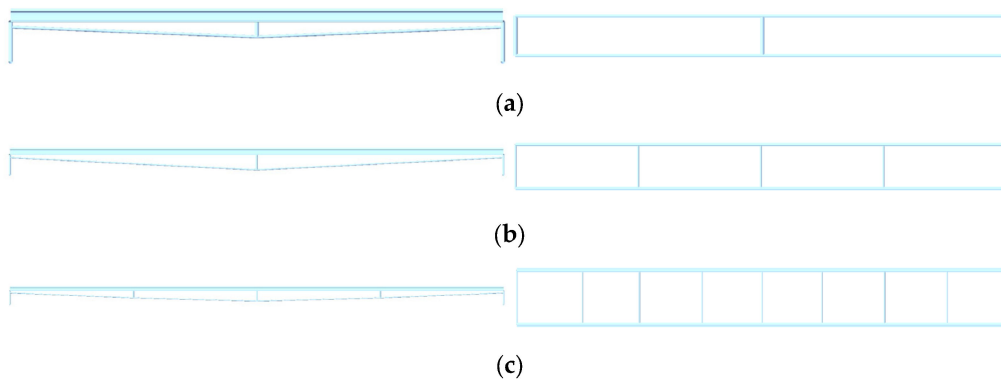
Figure 8. Finite element model of three spans. (**a**) 5 m span finite element model, (**b**) 10 m span finite element model, (**c**) 15 m span finite element model.

The method based on modal analysis needs to determine the order of the analyzed mode in advance, and this order can be determined according to the needs of calculation accuracy [8]. According to the actual structure situation, this paper chooses to use the first three fundamental frequencies of the structure to identify the dynamic load. The calculation results of the first three-order fundamental frequency of each structure under different working conditions are shown in Table 3.

Table 3. Summary of fundamental frequency calculation results.

	Vertical Vibration Frequency (Hz)			Transverse Vibration Frequency (Hz)		
Span (m)	**First Order** f_1	**Second Order** f_2	**Third Order** f_3	**First Order** f_1	**Second Order** f_2	**Third Order** f_3
5	16.40	65.57	117.80	13.95	28.64	69.57
10	4.18	15.90	30.40	3.77	10.68	17.81
15	2.1	8.18	12.57	1.70	27.62	48.07

Using the above fundamental frequency calculation results, combined with the measured data of the test line, the dynamic load of the AERORail can be identified.

3.2. Dynamic Load Identification

3.2.1. 5 m Span Dynamic Load Identification

For the acceleration and displacement data measured in the 5 m span under the working condition, we use an improved time domain method (ITDM) based on moments to be processed. Taking the speed of 20 km/h as an example, the measured mid-span acceleration signal is shown in Figure 9. As shown in Figure 9, the original signal sampling time is much longer than the actual loading time, and there is a long static time; the displacement signal has relatively strong noise, and it is necessary to use a certain filtering method to process the signal before subsequent analysis. The signal trough position is close to the acceleration signal peak position, which is the approximate time when the vehicle travels to the mid-span. In this paper, when processing the original signal, the dmey wavelet is used as the base wavelet to decompose and retain the real signal frequency band and remove the noise component to achieve filtering and noise reduction [24,25]. The wavelet decomposition level is set to 12, and the approximate components are retained, that is, the filtered displacement-time curve is obtained as shown in Figure 10.
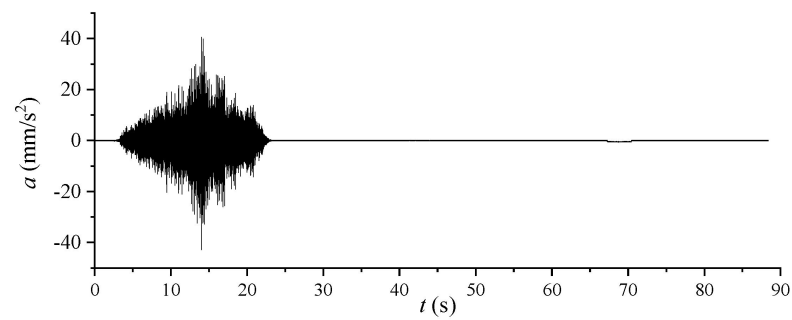
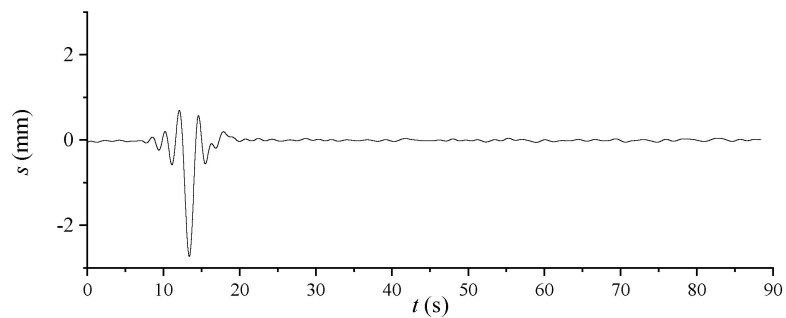**Figure 9.** Mid-span acceleration at 20 km/h.

Figure 10. Mid-span displacement signal after filtering at a speed of 20 km/h.

Utilizing the time domain identification method [26] and the filtered displacement signal in Figure 10, the actual moving speed and the loading start time and end time in the test can be identified; the acceleration signal actually used for calculation is intercepted at the two time points and is filtered as shown in Figure 11. Similarly, by using the time domain identification method and substituting parameters such as fundamental frequency and speed, the time-history curve of the vehicle-rail contact force can be identified (see Figure 12).
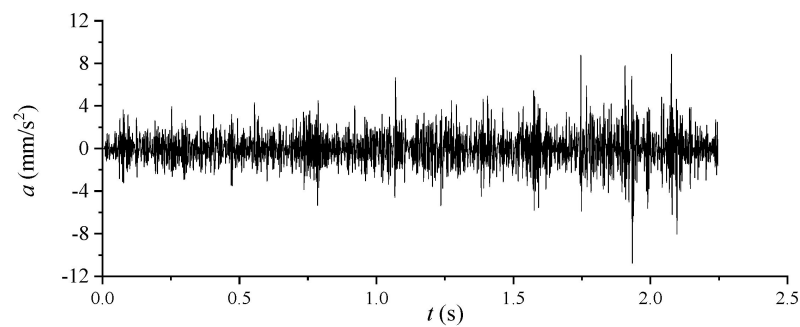

Figure 11. Filtered signal of mid-span acceleration at a speed of 20 km/h.
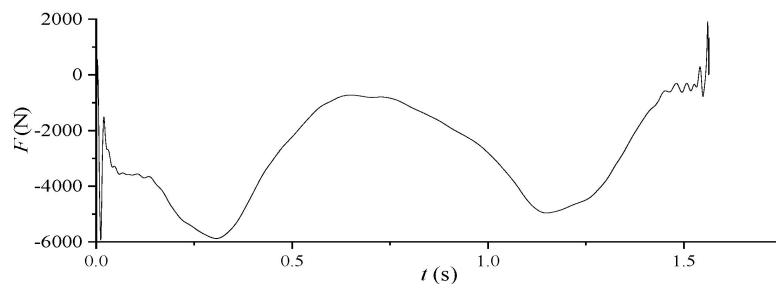

Figure 12. Identifying contact force at a speed of 20 km/h. Note: positive is pull and negative is press, the same as below.

The contact force-time curve after identification contains certain unreal data points, including the sudden change of the value at the start and end times or the crossing of the zero point. A contact force time-history curve that can be used for analysis can be obtained by removing the unreal data numerically.

Using the same method to process the data of the 5 m span under other speed conditions, the data curve is shown in Figure 13.
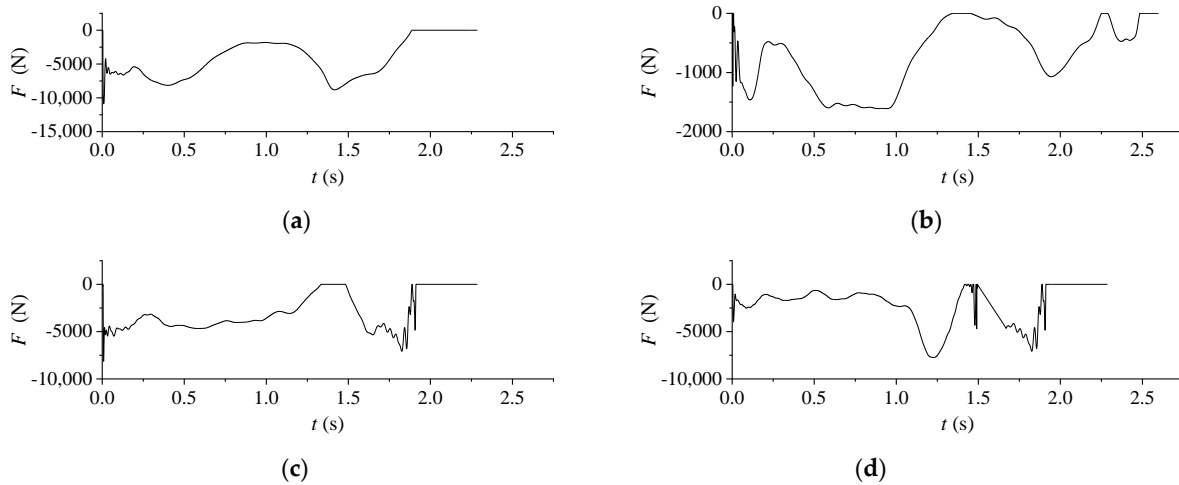
Figure 13. The contact force identification result of the 5 m span. (**a**) 5 km/h, (**b**) 10 km/h, (**c**) 15 km/h, (**d**) 20 km/h.

The results of the 5 m span generally show the following rules: (1) There are two absolute peak values of the contact force at the front and the back of the curve; (2) the contact force has a certain volatility; (3) there are data at the head and tail of the curve "Jitter"; (4) the recognition effect at low speed is not ideal, and there may be large errors. Among them, the existence of two contact force peaks may be caused by the fact that this identification method is equivalent to the equivalent treatment of the actual vehicle moving load; the contact force fluctuation is caused by the coupled vibration of the vehicle-rail, the stability of the algorithm and the fluctuation of the signal itself. The data fluctuation at the head and tail of the curve is caused by the sensitivity of the algorithm to the initial value condition.

From the contact force identification results in Figure 13, as the speed increases, the obvious point of the contact force usually appears in the second wave, and positive and negative changes appear, indicating that the relationship between the contact force and the vehicle speed in this span is affected by the passing time of the vehicle.

To further analyze the results of the 5 m span to draw more instructive general conclusions, the mean and maximum values of the above results are calculated, and the results are shown in Table 4:

Table 4. Statistical characteristics of the 5 m span contact force curve.

	5 km/h	10 km/h	15 km/h	20 km/h	25 km/h	Mean	Maximum Value
mean force (N)	4137.1	706.0	3470.1	2838.8	2241.0	2678.6	4137.1
max force (N)	8816.7	1610.5	7077.2	5876.3	7736.4	6223.4	8816.7

Note: data take absolute value, the same below.

Except for the abnormal data of 10 km/h, the data at other speeds have a statistical law that decreases with increasing vehicle speed on average. Specifically, it has the following three characteristics: the mean contact force decreases with increasing velocity in an

approximately linear trend; the maximum contact force fluctuates to a certain extent with the change in vehicle speed; there is a weak correlation between the statistical properties of the contact force curve and the vehicle speed.

3.2.2. 10 m Span Dynamic Load Identification

A similar method is used to process the acceleration and displacement data measured in the 10 m span, and some data are displayed according to the same method. The wavelet decomposition filtering method is used to filter the relevant displacement signals, and the dynamic deflection curves of the filtered 10 m span under different speed loads can be obtained. Using the time domain identification method and the filtered displacement signal, the actual movement and loading start and end times in the test are identified, and the acceleration signal actually used for calculation is intercepted.

After resampling, substitute the fundamental frequency data of the 10 m span in Table 3. Using the speed and time information obtained by identification and the filtered mid-span acceleration signal, the vehicle-rail contact force-time curve shown in Figure 14 can be identified and obtained.
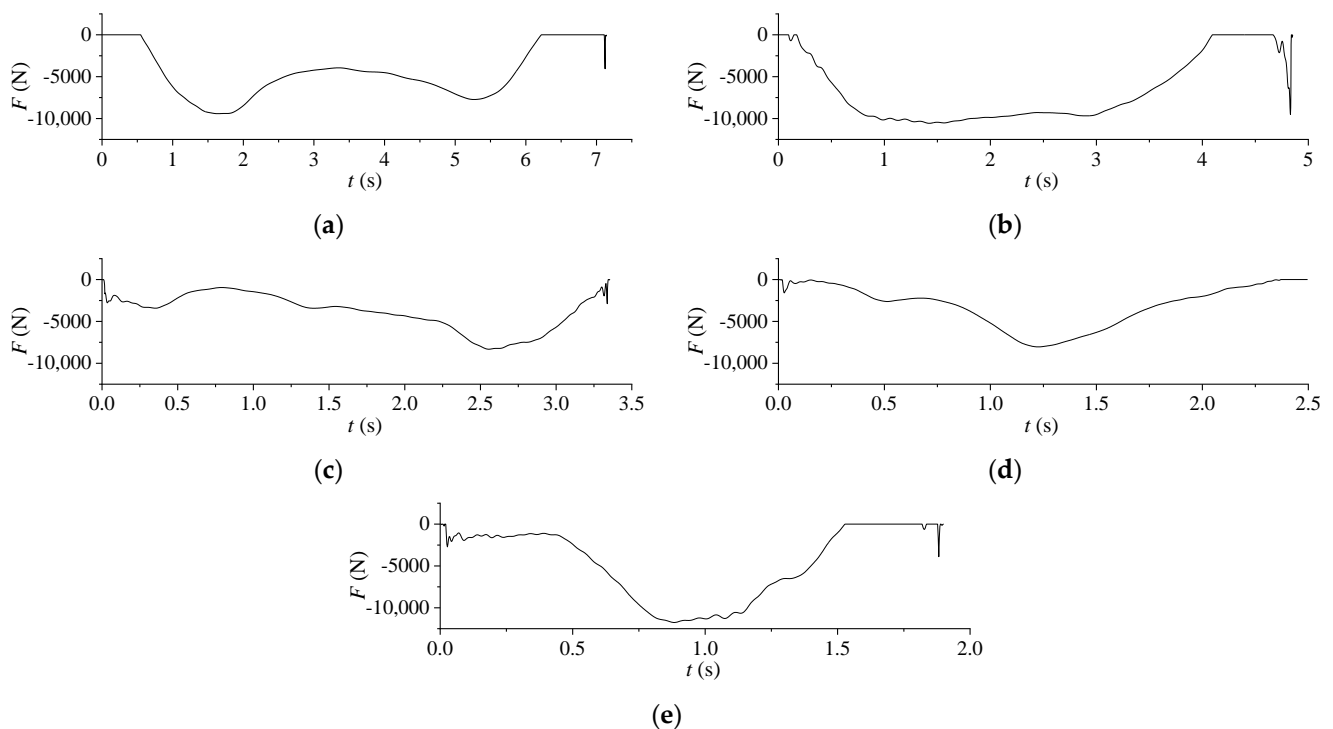
Figure 14. The contact force identification result of the 10 m span. (**a**) 5 km/h, (**b**) 10 km/h, (**c**) 15 km/h, (**d**) 20 km/h, (**e**) 25 km/h.

The general rules of the 10 m span results are as follows: (1) The two absolute peaks of the contact force at the front and the rear of the curve gradually disappear after the speed increases (over 10 km/h); (2) The contact force still has a certain volatility, but it is decreasing; (3) At higher speeds, a longer and gentler trough appears in the middle of the curve. The fusion of the two contact force peaks may be due to the time lag of the first impact generated by the contact force when the speed is faster and the second impact to advance instead, causing the vibration effects to overlap. This is caused by the stability of the algorithm and the fluctuation of the signal itself. When the span increases, the contact force has relative stability in the mean value and time of the impact force on the AERORail.

To further analyze the results of the 10 m span and draw more instructive general conclusions, the average and maximum values of the above results are also calculated, and the results are shown in Table 5.

Table 5. Statistical characteristic table of the 10 m span contact force curve.

	5 km/h	10 km/h	15 km/h	20 km/h	25 km/h	Mean	Maximum Value
mean force (N)	4520.0	6601.6	3809.1	3075.9	4586.8	4518.7	6601.6
max force (N)	9421.9	1,0573.0	8319.6	8043.7	1,1760.7	9623.8	1,1760.7

The data with a span of 10 m do not have obvious linear reduction characteristics, and the data volatility is obvious. Specifically, it has the following three characteristics: the average contact force fluctuates between 3800 and 4600 N with the speed change; the maximum contact force fluctuates to a certain extent with the change in vehicle speed; there is no obvious correlation between the statistical properties of the contact force curve and the vehicle speed.

3.2.3. 15 m Span Dynamic Load Identification

The acceleration and displacement data measured over the 15 m span are processed and displayed using similar methods for the 5 m and 10 m spans. Using the speed and time information obtained by identification and the filtered mid-span acceleration signal, the vehicle-AERORail contact force-time curve shown in Figure 15 can be identified and obtained.
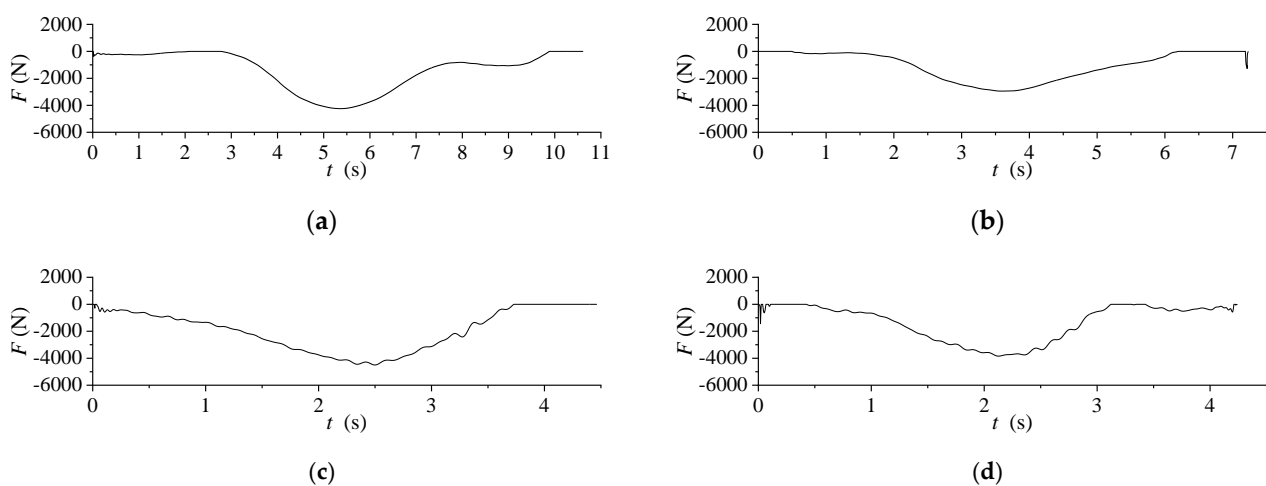
Figure 15. The contact force identification result of the 15 m span. (**a**) 5 km/h, (**b**) 10 km/h, (**c**) 15 km/h, (**d**) 20 km/h.

The results of the 15 m span show the following rules: (1) the curve shape is bowl-shaped with a gentle trough; (2) the contact force fluctuation has obvious high-frequency fluctuations at higher speeds (greater than or equal to 15 km/h) and (3) the contact force is small at low speed. The single-valley curve reflects that the peak of the contact force occurs when the moving force passes through the mid-span, rather than after the start or end of the loading; the fluctuation of the contact force is mainly contributed by the coupled vibration of the vehicle-rail, and the vibration effect gradually increases with increasing vehicle speed. Characteristics such as the mean value and the maximum value of the 10 m span are further analyzed and the results are shown in Table 6.

Table 6. Statistical characteristics of the 15 m span contact force curve.

	5 km/h	10 km/h	15 km/h	20 km/h	Mean	Maximum Value
mean force (N)	1354.3	1052.1	1901.9	1329.5	1409.4	1901.9
max force (N)	4246.2	2948.7	4501.0	3845.1	3885.3	4501.0

The data with a span of 15 m do not have obvious linear reduction characteristics, and the data volatility is obvious. Specifically, it has the following three characteristics: the average contact force fluctuates between 1300 and 1900 N with the speed change; the maximum value of the contact force fluctuates to a certain extent with the change in vehicle speed, but the average value is relatively stable; there is no obvious correlation between the statistical properties of the contact force curve and the vehicle speed. The above characteristics are basically consistent with the analysis conclusion of the 10 m span.

3.3. Analysis of Contact Force Law

According to the dynamic load analysis results of the three spans at different vehicle speeds, the obtained average contact force and maximum contact force were compared (see Figure 16).

(**a**)   (**b**)
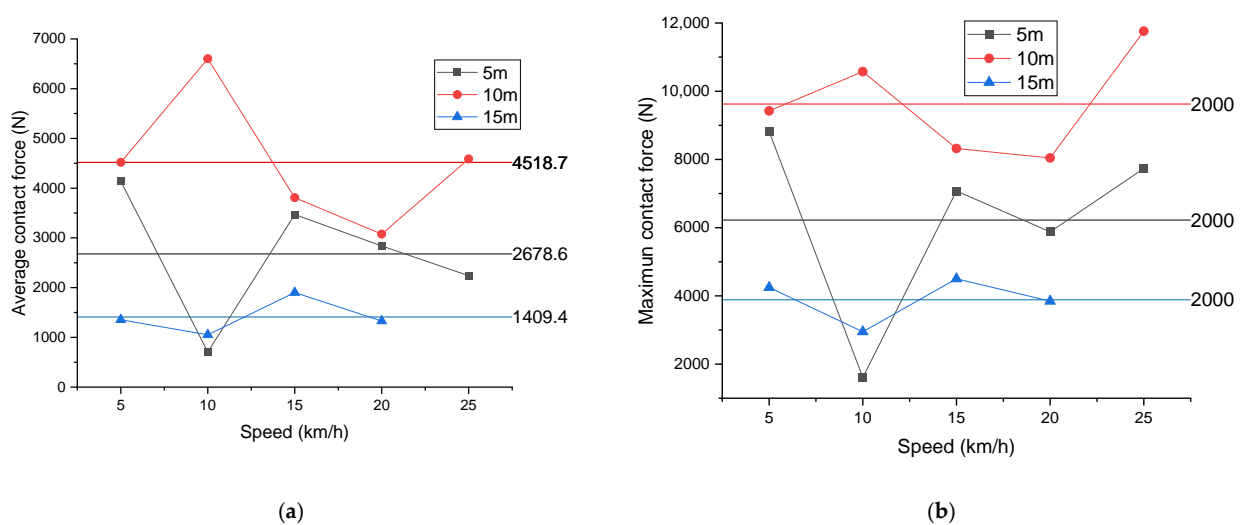
Figure 16. Relationship between vehicle speed and contact force. (**a**) Relationship between average contact force and vehicle speed, (**b**) Relationship between maximum contact force and vehicle speed.

Figure 16 shows that the contact force fluctuates with the change in vehicle speed, but as the span increases, the fluctuation of the contact force decreases significantly. The possible reasons for the analysis are related to the passing time of the vehicle and the influence of the track vibration caused by the passing of the vehicle.

When the speed is approximately 10 km/h, the fluctuation of the contact force is the most obvious. The current analysis may be that the corresponding span is related to the action time when the vehicle passes through. The speed of 10 km/h is approximately 3 m/s, and the coupled vibration of the track and the vehicle has an obvious influence.

Judging from the appearance time of the maximum contact force (see Figure 17), the small span is obviously affected by the short distance, and the contact force is basically the same as the vehicle passing time, but after the span greater than 10 m, the trend is more consistent, and it can be predicted that with the further increase in the span, the maximum contact force appearance time is more clearly correlated with the axle arrangement of vehicle and vehicle speed.
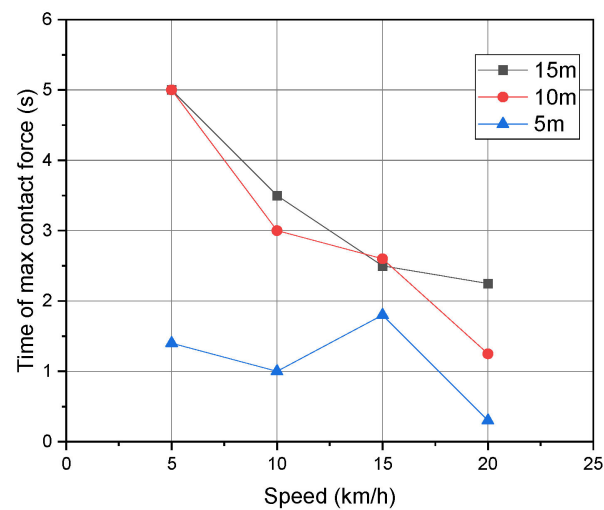
Figure 17. Time of maximum contact force.

4. Conclusions

Based on the modal test and the natural frequency determined, the contact force between the vehicle and rail of AERORail was studied under the vehicle load on different spans; the conclusions are listed as follows:

(1) Through the modal test and modal analysis results of the 30 m span and five-pole supported AERORail, the measured modal parameters and the finite element analysis modal parameters are compared. The results show that in some cases, the finite element analysis results can provide the modal parameters required for vertical vibration analysis, but in the lateral direction, the source of error between the two still needs to be deeply studied.

(2) By means of parameter identification, signal truncation, resampling and filtering, contact force calculation and error correction, the contact forces of different spans AERORail at different speeds can be obtained.

(3) In most cases, the statistical characteristics of the contact force, including the mean and maximum value, have no significant correlation with the velocity; in the case of small spans, the contact force will have two troughs, and in the larger spans and higher velocities, the contact force is a single-valley curve, indicating that the vibration of the structure, vehicle travel time, and wheel-axle contact are the main factors at small spans; when the speed is higher, the contact force curve will have more obvious fluctuations, but peak regularity is consistent.

(4) From the overall perspective of the three spans and five speeds, the contact force time-history curve has the following characteristics: the mean value of the contact force fluctuates in the range of 1800 N~4500 N with different working conditions; the maximum value of the contact force fluctuates in the range of 6000 N~11,000 N; there is no correlation between statistical characteristics such as the mean and maximum force and speed; at the start and end times, the contact force calculated by the identification algorithm is small and the fluctuation introduced by the algorithm is mainly reflected in the beginning and end of the contact force time-history curve area.

(5) Comprehensively considering the travel time, contact force and deformation law of vehicles passing through a span structure, it is determined that the maximum contact force is still directly generated by the upper moving load when the span is large, while the small span is significantly affected by the dynamic characteristics of the structure.

Institutional Review Board Statement: Not applicable.

Informed Consent Statement: Not applicable.

Data Availability Statement: The data used to support the findings of this study are included in the article.

Conflicts of Interest: The authors declare that they have no conflict of interest.

References

1. Li, F.; Liu, D.; Han, J.; Wang, J.L. Structure form of pretension string rail structure and application prospect. In *Structures and Architecture*; Cruz, P.J.S., Ed.; CRC Press: Boca Raton, FL, USA, 2010; pp. 1546–1553.
2. Why Hasn't Self-Anchored Suspension Bridge Been popularized. Available online: http://www.360doc.com/content/22/0426/18/5983216_1028428704.shtml (accessed on 26 April 2022).
3. The Arch Bridge Can Also Bend Downward. Available online: https://www.163.com/dy/article/DREID4S40516M7S1.html (accessed on 11 September 2018).
4. Li, F.Y.; Wu, P.; Lu, D. Experimental study on the cable rigidness and static behaviors of AERORail structure. *Steel Compos. Struct.* **2012**, *12*, 427–444. [CrossRef]
5. Lee, S.; Seo, M.; Baek, K.Y.; Jeong, J.; Kim, S.M.; Lee, J. Experimental study of two-way beam string structures. *Eng. Struct.* **2019**, *191*, 563–574. [CrossRef]
6. Ji, Y.C.; Kim, Y.J. State-of-the-art review of bridges under rail transit loading. *Proc. Inst. Civ. Eng.-Struct. Build.* **2019**, *172*, 451–466. [CrossRef]
7. Zhao, X.; Yan, S.; Xu, Z.; Wu, A. Research and Application of Beam String Structures. *Struct. Eng. Int.* **2015**, *25*, 26–33. [CrossRef]
8. Guangwei, Z.; Changzhao, Q.; Changping, C. Research on the Approximate Calculation Method of the Fundamental Frequency and Its Characteristics on a Tensioned String Bridge. *Processes* **2022**, *10*, 126.
9. Hartweg, S.; Heckmann, A. Moving loads on flexible structures presented in the floating frame of reference formulation. *Multibody Syst. Dyn.* **2016**, *37*, 195–210. [CrossRef]
10. Lee, K. Numerical analysis for dynamic contact between high-speed wheel and elastic beam with Coulomb friction. *Int. J. Numer. Methods Eng.* **2009**, *78*, 883–900. [CrossRef]
11. Lee, K. A numerical method for dynamic analysis of vehicles moving on flexible structures having gaps. *Int. J. Numer. Methods Eng.* **1997**, *40*, 511–531. [CrossRef]
12. Zhao, X.W.; van der Heijden, G.H.M. Dynamics and stability of slender structures carrying a moving load or mass. *Procedia Eng.* **2017**, *199*, 2609–2614. [CrossRef]
13. Xiao, X.; Chen, Y.; Shen, W.; Zhu, H. Vibration control of stress ribbon bridges subjected to moving vehicles. *Struct. Control Health Monit.* **2021**, *28*, e2835. [CrossRef]
14. Fukada, S. Serviceability of stress ribbon bridges with external tendons. *Proc. Inst. Civ. Eng.-Bridge Eng.* **2015**, *168*, 123–138. [CrossRef]
15. Zhang, Y.; Pu, W.; Zhang, Q.; Liu, K.; Dong, H. Effect of Ground Motion Orientation on Seismic Responses of an Asymmetric Stress Ribbon Pedestrian Bridge. *Adv. Civ. Eng.* **2022**, *2022*, 1278314. [CrossRef]
16. Li, F.; Wu, P.; Liu, D. Application of Virtual Prototyping to Simulation of Vehicle-rail Coupling of AERORail Structure. *J. Tongji Univ. (Nat. Sci.)* **2012**, *40*, 1287–1293.
17. Peng, S. Study on static characteristics of a new pretensioned pretensioned string AERORrail structure. In *Department of Bridge Engineering*; Tongji University: Shanghai, China, 2017.
18. Yu, C. Study on dynamic characteristics of a new pretensioned string AERORrail structure. In *Department of Bridge Engineering*; Tongji University: Shanghai, China, 2018.
19. Li, K.R. Inferred cable force of the beam-string structure based on finite element simulation and simplified method of cable force test using frequency method. *Sichuan Build. Sci.* **2021**, *47*, 35–39.
20. Yan, Z.; Teng, S.; Luo, W.; Bassir, D.; Chen, G. Bridge Modal Parameter Identification from UAV Measurement Based on Empirical Mode Decomposition and Fourier Transform. *Appl. Sci.* **2022**, *12*, 8689. [CrossRef]
21. Lorenzoni, F.; De Conto, N.; da Porto, F.; Modena, C. Ambient and free-vibration tests to improve the quantification and estimation of modal parameters in existing bridges. *J. Civ. Struct. Health Monit.* **2019**, *9*, 617–637. [CrossRef]
22. Zulkifli, E.; Widarda, D.R. Modal parameters identification of light rail bridges. *IOP Conf. Ser. Mater. Sci. Eng.* **2019**, *669*, 012027. [CrossRef]
23. Law, S.S.; Chan, T.H.; Zeng, Q.H. Moving force identification: A time domain method. *J. Sound Vib.* **1997**, *201*, 1–22. [CrossRef]
24. Xue, Z.; Cheng, X.; Li, L.; Zhang, X.; Li, D. Study on the separation overlapping spectrum by "dmey" wavelet transformation and genetic algorithms. *J. Chongqing Univ. Arts Sci.* **2014**, *33*, 104–106+111.

25. Grobbelaar, M.; Phadikar, S.; Ghaderpour, E.; Struck, A.F.; Sinha, N.; Ghosh, R.; Ahmed, M.Z.I. A Survey on Denoising Techniques of Electroencephalogram Signals Using Wavelet Transform. *Signals* **2022**, *3*, 577–586. [CrossRef]
26. Yang, J.; Hou, P.; Yang, C.; Zhang, Y. Study on the Method of Moving Load Identification Based on Strain Influence Line. *Appl. Sci.* **2021**, *11*, 853. [CrossRef]